NANO LETTERS

pubs.acs.org/NanoLett Letter

Experimental and Computational Study of the Orientation Dependence of Single-Crystal Ruthenium Nanowire Stability

Maxwell A. L'Etoile, Baoming Wang, Quintin Cumston, Andrew P. Warren, James C. Ginn, Katayun Barmak, Kevin R. Coffey, W. Craig Carter, and Carl V. Thompson*

Cite This: https://doi.org/10.1021/acs.nanolett.2c03529 Read Online

ACCESS | Metrics & More | Article Recommendations | Supporting Information

ABSTRACT: Single-crystal nanowires are of broad interest for applications in nanotechnology. However, such wires are subject to both the Rayleigh−Plateau instability and an ovulation process that are expected to lead to their break up into particle arrays. Single crystal Ru nanowires were fabricated with axes lying along different crystallographic orientations. Wires bound by equilibrium facets along their length did not break up through either a Rayleigh−Plateau or ovulation process, while wires with other orientations broke up through a combination of both. Mechanistic insight is provided using a level-set simulation that accounts for strongly anisotropic surface energies, providing a framework for design of morphologically stable nanostructures.

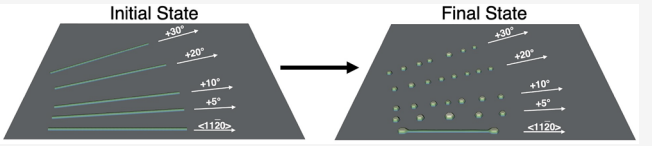

KEYWORDS: *nanowires, Rayleigh instability, surface energy anisotropy, solid-state dewetting, agglomeration*

Nanowires and other fabricated nanostructures are unstable and will undergo morphological evolution to energy-minimizing shapes. For solid nanostructures, this evolution is typically governed by surface diffusion and is accelerated as temperature is increased.[1−5] In isotropic systems, this behavior is described by the Mullins equation,[6] which states that the velocity of an evolving surface is proportional to the surface Laplacian of the product of surface energy density and curvature, $\gamma\cdot\kappa$. Thin films deposited on substrates, and structures patterned from thin films, agglomerate to form particles while remaining in the solid state.[7−10] The energy that drives this solid-state dewetting process increases as the dimensions of nanostructures such as wires and films are made smaller, so that rapid solid-state dewetting occurs at lower temperatures.[1]

Isotropic materials that are in cylindrical form are expected to break up into particles through a process first described for liquid jets by Plateau[11] and analyzed by Lord Rayleigh.[12] Rayleigh's instability analysis showed that a cylinder with isotropic surface energy and radius R_0 will decompose through growth of perturbations having a wavelength greater than $\lambda_{crit} = 2\pi R_0$. Nichols and Mullins showed that this result also holds for solid cylinders with isotropic surface energy that evolve through capillary-driven surface diffusion.[13] They further showed that when the shape evolves through surface diffusion, the fastest-growing perturbation has wavelength $\lambda_{max} = 2\sqrt{2}\pi R_0$, such that the resulting particles tend to be spaced at this distance. The analysis of Nichols and Mullins has been extended to the case of wires on substrates which they partially wet with contact angles between 0 and 180°.[14] Nichols also showed that the ends of unperturbed wires could repeatedly pinch off in a process he called ovulation.[15] Compared to Rayleigh-like break up, ovulation results in larger particles which are formed sequentially, rather than simultaneously.

Santala and Glaeser artificially created wire-shaped voids with lengths much greater than their average diameter in single crystals of sapphire and showed that, when the samples were annealed, the long voids broke up into more axisymmetric voids, as expected for a Rayleigh-like instability.[16] However, they found that the rate of this Rayleigh-like break up and the spacing and size of the voids that formed were strongly affected by the crystallographic orientation of the axis of the wire-shaped voids, even when their initial cross-sectional areas were the same. More recently, Kim and Thompson showed that Ni wires formed from patterned single-crystal films broke up through a Rayleigh-like process that was also strongly dependent on the crystallographic orientation of the wire axis.[17]

While Rayleigh-like breakup of wires with isotropic properties can be readily analyzed and simulated, the effects of anisotropy are much harder to treat, especially when faceted surfaces develop. Cahn originally studied the effects of anisotropy which was rotationally isotropic about the axis of a cylinder,[18] while Gurski and McFadden more recently examined the stability of wires with cubic anisotropy.[19] However, a general understanding of the effects of anisotropy on the stability of wires has not emerged.

Received: September 6, 2022
Revised: December 5, 2022

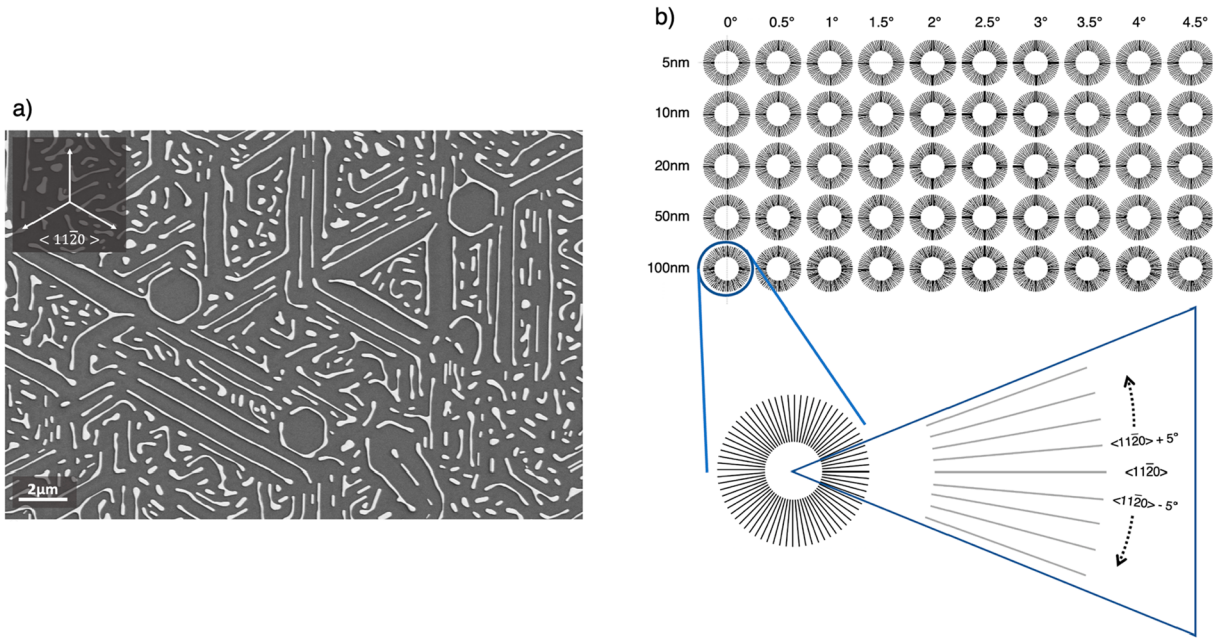

Figure 1. (a) Representative view of a 5 nm-thick (0001)Ru film annealed at 950 °C for 3 h. Solid state dewetting led to an intermediate state composed of wire-like features aligned along ⟨11$\bar{2}$0⟩ orientations. (b) Lithographic pattern used to explore the behaviors of strips of different widths and crystallographic orientations. This pattern allows half-degree angular resolution for a given strip width.

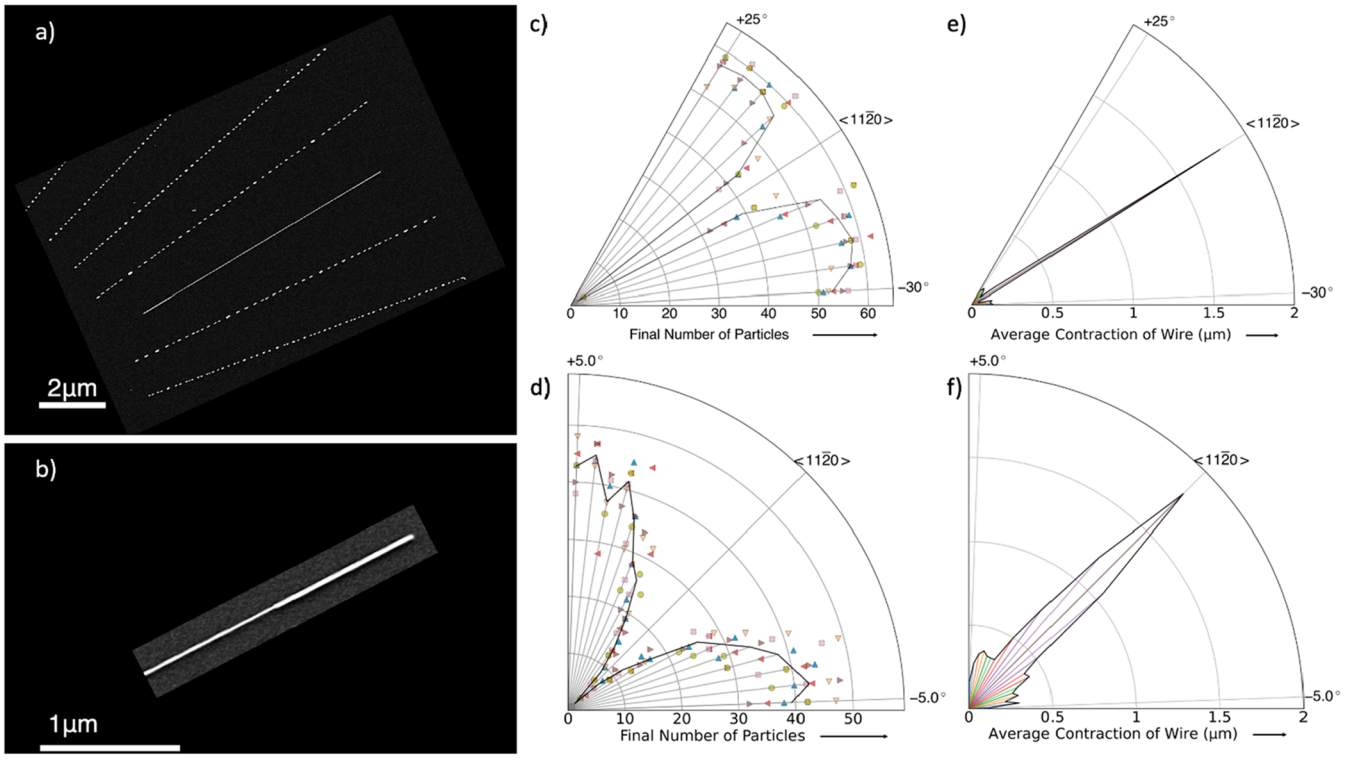

Figure 2. Summary of experimental results for patterned 20 nm-wide lines (see Figure 4 for postanneal cross-section). (a) Representative image of dewetted wires after annealing at 950 °C for 3 h. The wire aligned along a ⟨11$\bar{2}$0⟩ direction has not broken up, but it has shortened significantly. Lines with other orientations have broken up but have not significantly shortened. (b) Close up of the end of the stable wire, highlighting how mass from the retracting end has accumulated in a sharply defined thicker segment. (c and d) Plots of the average number of particles as a function of wire orientation, with part c showing the whole range in 5° increments and part d focusing on lines lying between ±5° around the central cusp in half-degree increments. Points show results for individual wires and the line indicates the average. (e and f) Plots of the average length contraction as a function of orientation, at 5° and 0.5° increments, respectively. For unstable wires, length contraction is defined as the difference between the as-patterned length and the distance between the two outermost particles.

https://doi.org/10.1021/acs.nanolett.2c03529
Nano Lett. XXXX, XXX, XXX−XXX

In this paper, we report on detailed studies of the breakup of single-crystal Ru nanowires with axes aligned along different crystallographic directions. We find very pronounced effects of crystalline anisotropy on the Rayleigh-like break up of these wires and further show that break up of wires bound by equilibrium facets along their length is fully suppressed. We show that key features of these experiments are reproduced using a new level-set simulation of dewetting that captures the effects of anisotropic properties.[20]

To fabricate test structures for these experiments, single-crystal 5-nm-thick (0001) Ru films were grown on (0001) sapphire substrates using UHV DC magnetron sputtering, as detailed in ref 21. For the films used here, the substrates were held at 500 °C during deposition. Post deposition, but prior to lithographic patterning, samples were step annealed in a vacuum furnace. The furnace tube was pumped down to 20 mTorr, and then Ar/H_2 flowed at 16 sccm to provide a pressure of 100 mTorr during the annealing process. The furnace was then brought to 400 °C and held for 1 h. The temperature was subsequently increased in 100 °C steps and held for 1 h at each step until reaching and being held at 700 °C for 30 min. The temperature was then stepped down by 200 °C every 2 h until reaching 400 °C, at which point the samples were allowed to cool to room temperature naturally. After this step anneal, no significant dewetting was observed away from the edges of the films, where lithographic patterning was performed. Films deposited and processed under these conditions were confirmed to be single-crystalline using XRD, as in reference.[21] Ru was chosen both because of potential technological applications[22,23] and because its HCP crystal structure seemed likely to yield behaviors which differed from those of well-studied FCC metals, such as Ni,[24−26] and diamond cubic materials, such as silicon,[27,28] in interesting ways.

For dewetting experiments, continuous films were annealed in a tube furnace through which 95%Ar/5%H_2 was flowing at 2300 sccm. The inner diameter of the furnace tube was 20.5 mm. It was found that annealing at 950 °C for 3 h resulted in solid-state dewetting to an intermediate state consisting of elongated wire-like features and hexagonal rings aligned along $\langle 11\bar{2}0\rangle$ directions, as shown in Figure 1a. This result suggested that wires with these alignments were likely to be resistant to Rayleigh-like breakup.

With this information, e-beam lithography was used to pattern radial arrays of nominally 10 μm long, 20 nm wide strips of Ru from 5 nm thick films. Details of the lithographic patterning process are given in the Supporting Information (see discussion of process A in the Supporting Information and Figure SI1). The layout of the patterned sample is shown in Figure 1b. Each radial wire array contained 72 wires, each offset by 5° from its neighbors. The wafer was patterned with several replicate subsamples, each patterned with different e-beam exposure dosages to ensure at least one well-resolved subsample. Each subsample contained 10 such arrays, the first with 6 strips aligned along $\langle 11\bar{2}0\rangle$ directions and each subsequent array being increasingly offset from this in 0.5° increments, resulting in half-degree angular resolution overall.

After lithographic patterning, the sample was annealed at 915 °C for 3 h and subsequently studied using high-resolution scanning electron microscopy (HRSEM). During annealing, the sides of the strips retracted to form wires and then most of the wires broke up into particles. The results from the best-resolved subsample, summarized in Figure 2, are striking. Wires aligned along $\langle 11\bar{2}0\rangle$ directions were seen to be much more stable than wires with other orientations, with most remaining entirely intact and contracting significantly in length, while those offset by even a few degrees underwent negligible length contraction and broke up into dozens of particles. The dependence of both the number of particles and length contraction on strip orientation is highly nonlinear, with sharp cusps at stable orientations and the majority of the effect being saturated within a few degrees of offset.

To explore the mechanisms leading to this very strongly orientation-dependent behavior, a different lithography process (see discussion of process B in the Supporting Information and Figure SI2) was used to pattern the same starburst structure as above but with strips that were initially ∼70 nm wide. These wider samples were annealed under the same conditions as above in short time increments and examined using HRSEM. The sides of the strips rapidly retracted to form wires, and these wires then displayed behavior similar to that described above. The larger wire diameter led to slower evolution and to features that were more readily resolved in HRSEM images. Note that wires of all orientations have nominally identical cross-sectional areas, and in the isotropic case, would be expected to break up at the same rate to form particles with the same size and spacing. As previous work on single-crystal wire stability[17] would suggest, the development of a Rayleigh-like instability is evident for all but the wires aligned along $\langle 11\bar{2}0\rangle$ directions. Figure 3a shows

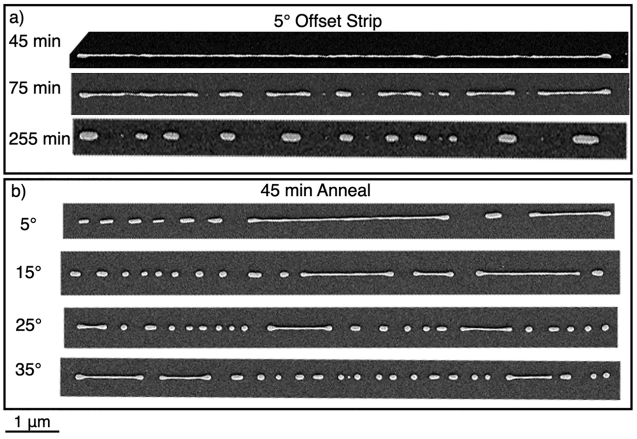

Figure 3. (a) Images at selected times showing the evolution of a wire with 5° offset relative to a $\langle 11\bar{2}0\rangle$ direction, showing mostly Rayleigh-like breakup. (b) Wires with selected offsets after 45 min of annealing showing evidence of both Rayleigh-like and ovulation behavior. Note that breakup of the 5° wires in both parts a and b leads to a significantly greater characteristic spacing than the wires with larger offset, which share similar particle spacings.

the development of such an instability on a wire offset from $\langle 11\bar{2}0\rangle$ by 5°. The wavelength of this instability is relatively large and leads to large particles at correspondingly large spacings. For larger angular offsets (Figure 3b), the periodicity of the breakup, and thus the final spacing of the particles, was significantly smaller. In all cases, the Rayleigh instability develops with some irregularity along the length of the wire. Therefore, at intermediate stages, long segments of unbroken wire coexist with fully formed particles. These particles are observed to have relatively broad distributions of sizes and spacings.

A cross-sectional Transmission Electron Microscope (TEM) image of a stable Ru wire is shown in Figure 4a. This image shows that the wire is bound by specific low index facets. The wire was sectioned such that the image plane was normal to the

https://doi.org/10.1021/acs.nanolett.2c03529
Nano Lett. XXXX, XXX, XXX−XXX

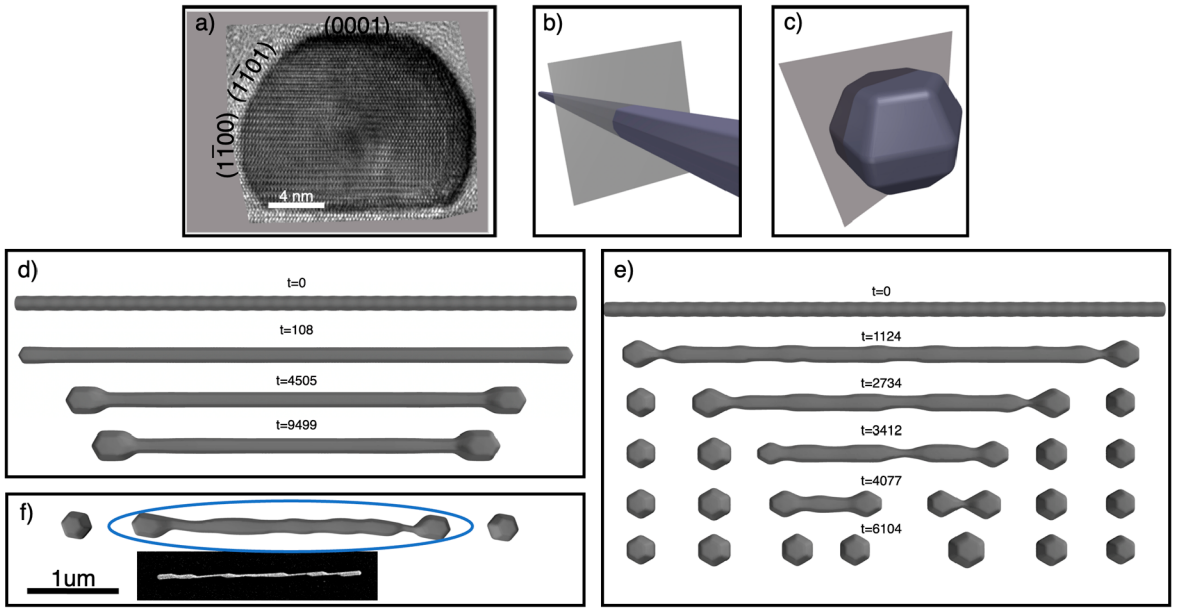

Figure 4. (a) Cross-section of a stable wire obtained using focused ion beam sectioning and transmission electron microscopy. (b) Illustration of the TEM image plane relative to the axis of the wire and (c) the Wulff shape assumed in our simulations, with the relevant cross-sectional plane from parts a and b shown in gray. (d) Stable (0° offset) wire undergoing length contraction with no ovulation or Rayleigh instability. (e) Simulation of a wire offset from the stable orientation by 30°. Both Rayleigh-like and ovulation modes are evident. (f) Snapshot from a 10° offset simulation matching the behavior of a segment of a 6° offset wire from experiment. The values for time given in the simulations can be compared across figures but are not directly comparable to experiments; see Supporting Information for a discussion of units in the simulation. Full videos of all simulations are also available in the Supporting Information.

axis of the wire, Figure 4b. The observed facets correspond well with equilibrium facets on the Wulff shape[29] generated from DFT calculations using the three lowest energy planes of Ru.[30] This supports the understanding that the facets seen in the cross-sectional image lie parallel to the axis of the wire. The Wulff shape shown in Figure 4c has been generated with slightly rounded corners and edges to match the experimental observation. A wire bound by facets along its length is expected to be resistant to a Rayleigh-like break up because of the large energy penalty associated with growth of perturbations of the stable facets. This having been said, we have found that this effect is surprisingly strong, even in the presence of rounded corners and edges.

To better understand the phenomenological observations shown above, we used our recently developed level-set simulation method[20] to simulate the evolution of finite, cylindrical, free-standing Ru wires, i.e. effects of the substrate were ignored in these simulations. In dimensionless units, these wires had length 379, and radius 5, with an initial sinusoidal perturbation of wavelength 10 and amplitude 0.1 to provide some surface roughness. Simulations were conducted using a Cahn−Hoffman vector[31,32] $\vec{\xi}(\hat{n})$, corresponding to the Wulff shape shown in Figure 4b, see the Supporting Information for more details. The role of $\vec{\xi}(\hat{n})$ in encoding surface energy anisotropy in our simulations is discussed in detail in.[20] In short, $\vec{\xi}(\hat{n})$ is a vector-valued quantity derived from a material's surface energy $\gamma(\hat{n})$. Taking the divergence of $\vec{\xi}(\hat{n})$ along an object's surface yields its weighted mean curvature, denoted κ_γ,[31,33] which can be used as a replacement for the product $\kappa \cdot \gamma$ in the isotropic Mullins equation. Simulations were conducted for wires offset from $\langle 11\bar{2}0\rangle$ by 5°, 10°, 20°, and 30°, in the same plane as the experiment. For computational efficiency, only the top half of the wires were simulated, and mirror boundary conditions were used. A wire aligned along the stable orientation was simulated as well. As in the experiments, the simulated wire aligned along the $\langle 11\bar{2}0\rangle$ contracted significantly in length with no breakup or evidence of a Rayleigh-like instability. In the other simulations, ovulation[15] of the wires' ends led to greatly reduced contraction in length—measured as the difference between the initial length of the wire and the span between the outer edges of the particles that formed at the ends once evolution was complete, see Figure 4d. As in the experiments, for all nonzero offsets, Rayleigh instabilities develop along the length of the wire, with the instability on the 5° offset wire having a much larger wavelength. Rayleigh-like pinch-off does not occur everywhere at the same time, so long segments coexist with fully broken-up regions, as in experiments. The ends of the long segments begin to ovulate as they retract so that ovulation significantly contributes to the overall breakup process; Figure 4e shows an example. Qualitative comparisons of simulation snapshots and experimental images suggest that the simulations are faithfully capturing many details of the experimental system, as exemplified in Figure 4f. These comparisons also drew attention to experimental images in which ovulation appears to be occurring or to have recently occurred, including at the ends of long segments created by Rayleigh-like pinch-off. From such comparisons, we conclude that both Rayleigh-like breakup and ovulation contribute to the breakup of Ru nanowires and that it is the combination of Rayleigh-like pinch-off and ovulation that lead to the relatively broad distributions of particle sizes and spacings observed in both the simulations and experiments. The importance of ovulation, particularly ovulation acting on long segments created from initially Rayleigh-like behavior, is an unexpected result that challenges the idea that the Rayleigh instability is the dominant mechanism of breakup for long wires. It is especially noteworthy that wires bound by facets along their length are stable with respect to both Rayleigh breakup and ovulation. The simulations reproduce the experimentally

https://doi.org/10.1021/acs.nanolett.2c03529
Nano Lett. XXXX, XXX, XXX−XXX

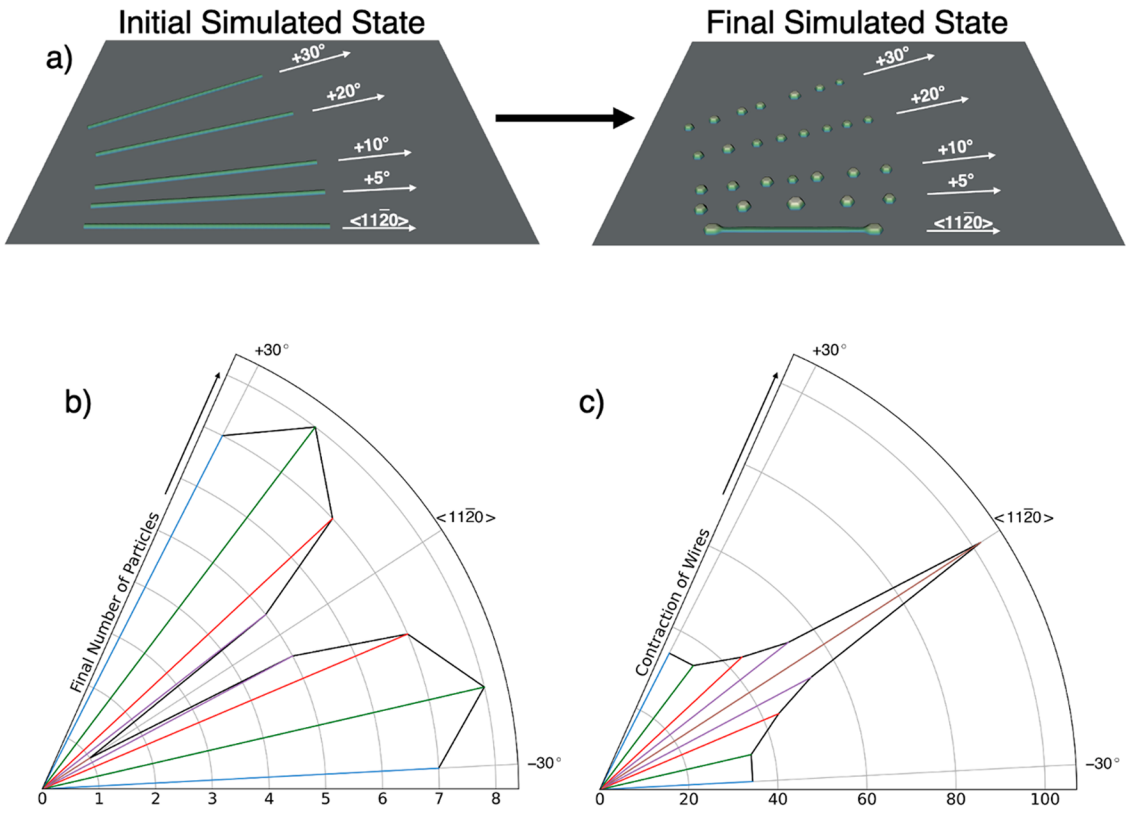

Figure 5. (a) Initial and final states of the simulated wires. The gray plane indicates the mirror plane across which mirror boundary conditions were implemented, which is equivalent to a 90° effective contact angle. (b and c) Simulation results showing analogous plots to Figure 2, parts c and e. Simulated breakup periodicity and length contraction depend on orientation in a way that closely parallels experimental results.

observed orientation dependence of both the retraction distance and the number of particles into which a wire breaks up (Figure 2), as shown in Figure 5. Although our simulations recover the orientation-dependent breakup behavior with a high degree of fidelity, one detail that is not fully recovered is the elongated "heads" of dewetting stable wires. We suspect that anisotropic surface mobility may contribute to this behavior, and this is a topic of ongoing investigation. Because of computational limitations, the length-to-width ratio of the simulated wires presented in this paper was significantly smaller than that of the experimental wires. To validate that the behavior observed in these simulations was not dominated by length-dependent effects, one simulation was run for a wire of initial diameter 10 and length 779 with an offset of 30°; as summarized in the Supporting Information, Figure SI3. Videos of the five primary simulations are also included in the Supporting Information.

In summary, understanding the morphological stability of nanowires with strongly anisotropic properties has proven to be a challenging problem for some time. In experiments using single-crystal Ru nanowires aligned along different crystallographic axes, we have shown that wires bound by facets along their length are stable with respect to Rayleigh-like breakup and ovulation, while wires with nominally the same cross-sectional dimensions but different orientations breakup through an interplay of both mechanisms. We show that a level-set simulation that accounts for the effects of strong surface energy anisotropy reproduces the behavior seen in experiments. These results point to the importance of crystallographic alignment in producing morphologically stable nanostructures and provide a framework for analysis and prediction of morphological stability that accounts for strong crystalline anisotropy.

■ ASSOCIATED CONTENT

Supporting Information

The Supporting Information is available free of charge at https://pubs.acs.org/doi/10.1021/acs.nanolett.2c03529.

Video S1: Simulation of a wire with the stable orientation (MP4)

Video S2: Simulation of a wire with a 5° offset from the stable orientation (MP4)

Video S3: Simulation of a wire with a 10° offset from the stable orientation (MP4)

Video S4: Simulation of a wire with a 20° offset from the stable orientation (MP4)

Video S5: Simulation of a wire with a 30° offset (MP4)

Detailed discussion (with schematics) of lithographic patterning processes used, discussion of additional simulation details and parameters (including surface energy anisotropy and level-set smoothing), and video captions from all simulations (PDF)

■ AUTHOR INFORMATION

Corresponding Author

Carl V. Thompson − *Department of Materials Science and Engineering, Massachusetts Institute of Technology, Cambridge, Massachusetts 02139, United States;* orcid.org/0000-0002-0121-8285; Email: cthomp@mit.edu

https://doi.org/10.1021/acs.nanolett.2c03529
Nano Lett. XXXX, XXX, XXX−XXX

Authors

Maxwell A. L'Etoile − *Department of Materials Science and Engineering, Massachusetts Institute of Technology, Cambridge, Massachusetts 02139, United States;* orcid.org/0000-0001-6647-9198

Baoming Wang − *Department of Materials Science and Engineering, Massachusetts Institute of Technology, Cambridge, Massachusetts 02139, United States*

Quintin Cumston − *Department of Materials Science and Engineering and Department of Physics, University of Central Florida, Orlando, Florida 32816, United States*

Andrew P. Warren − *Plasmonics, Inc., Orlando, Florida 32826, United States*

James C. Ginn − *Plasmonics, Inc., Orlando, Florida 32826, United States*

Katayun Barmak − *Department of Applied Physics and Applied Mathematics, Columbia University, New York, New York 10027, United States*

Kevin R. Coffey − *Department of Materials Science and Engineering and Department of Physics, University of Central Florida, Orlando, Florida 32816, United States*

W. Craig Carter − *Department of Materials Science and Engineering, Massachusetts Institute of Technology, Cambridge, Massachusetts 02139, United States*

Complete contact information is available at: https://pubs.acs.org/10.1021/acs.nanolett.2c03529

Notes

The authors declare no competing financial interest.

■ ACKNOWLEDGMENTS

This work was supported by NSF Grant Nos. DMR-1505947, EECS-1740274, ECCS-1740228, and EECS-1740270, Semiconductor Research Corporation Task Nos. 2764.001, 2764.002, and 2764.003, and the Air Force Office of Scientific Research Grants AFOSR FA9550-18-1-0063 and FA9550-19-1-0156. N. T. Nuhfer and K. Sentosun are thanked for the early effort in plasma FIB patterning of the nanowires.

■ REFERENCES

(1) Gadkari, P. R.; Warren, A. P.; Todi, R. M.; Petrova, R. V.; Coffey, K. R. Comparison of the Agglomeration Behavior of Thin Metallic Films on SiO2. *J. Vac. Sci. Technol. Vac. Surf. Films* **2005**, *23*, 1152.

(2) Giermann, A. L.; Thompson, C. V. Solid-State Dewetting for Ordered Arrays of Crystallographically Oriented Metal Particles. *Appl. Phys. Lett.* **2005**, *86*, 121903.

(3) Danielson, D. T.; Sparacin, D. K.; Michel, J.; Kimerling, L. C. Surface-Energy-Driven Dewetting Theory of Silicon-on-Insulator Agglomeration. *J. Appl. Phys.* **2006**, *100*, 083507.

(4) Bussmann, E.; Cheynis, F.; Leroy, F.; Müller, P.; Pierre-Louis, O. Dynamics of Solid Thin-Film Dewetting in the Silicon-on-Insulator System. *New J. Phys.* **2011**, *13*, 043017.

(5) Rabkin, E.; Amram, D.; Alster, E. Solid State Dewetting and Stress Relaxation in a Thin Single Crystalline Ni Film on Sapphire. *Acta Mater.* **2014**, *74*, 30.

(6) Mullins, W. W. Theory of Thermal Grooving. *J. Appl. Phys.* **1957**, *28*, 333.

(7) Srolovitz, D. J.; Goldiner, M. G. The Thermodynamics and Kinetics of Film Agglomeration. *JOM* **1995**, *47*, 31.

(8) Thompson, C. V. Solid-State Dewetting of Thin Films. *Annu. Rev. Mater. Res.* **2012**, *42*, 399.

(9) Leroy, F.; Borowik, Ł.; Cheynis, F.; Almadori, Y.; Curiotto, S.; Trautmann, M.; Barbé, J. C.; Müller, P. How to Control Solid State Dewetting: A Short Review. *Surf. Sci. Rep.* **2016**, *71*, 391.

(10) Ye, J.; Zuev, D.; Makarov, S. Dewetting Mechanisms and Their Exploitation for the Large-Scale Fabrication of Advanced Nanophotonic Systems. *Int. Mater. Rev.* **2019**, *64*, 439.

(11) Plateau, M. T. On the Recent Theories of the Constitution of Jets of Liquid Issuing from Circular Orifices. *London Edinb. Dublin Philos. Mag.* **1856**, *12*, 286.

(12) Rayleigh, Lord On The Instability Of Jets. *Proc. London Math. Soc.* **1878**, *s1−10*, 4.

(13) Nichols, F. A.; Mullins, W. W. Surface- (Interface-) and Volume Diffusion Contributions to Morophological Changes Driven by Capillarity. *Trans. Metall. Soc. AIME* **1965**, *233*, 1840.

(14) Mccallum, M. S.; Voorhees, P. W.; Miksis, M. J.; Davis, S. H.; Wong, H. Capillary Instabilities in Solid Thin Films: Lines. *J. Appl. Phys.* **1996**, *79*, 7604.

(15) Nichols, F. A. On the Spheroidization of Rod-Shaped Particles of Finite Length. *J. Mater. Sci.* **1976**, *11*, 1077.

(16) Santala, M. K.; Glaeser, A. M. Surface-Energy-Anisotropy-Induced Orientation Effects on Rayleigh Instabilities in Sapphire. *Surf. Sci.* **2006**, *600*, 782.

(17) Kim, G. H.; Thompson, C. V. Effect of Surface Energy Anisotropy on Rayleigh-like Solid-State Dewetting and Nanowire Stability. *Acta Mater.* **2015**, *84*, 190.

(18) Cahn, J. W. Stability of Rods with Anisotropic Surface Free Energy. *Scr. Metall.* **1979**, *13*, 1069.

(19) Gurski, K. F.; McFadden, G. B. The Effect of Anisotropic Surface Energy on the Rayleigh Instability. *Proc. R. Soc. London Ser. Math. Phys. Eng. Sci.* **2003**, *459*, 2575.

(20) L'Etoile, M. A., Thompson, C. V.; Carter, W. C. A Level-Set Method for Simulating Dewetting in Systems with Strong Crystalline Anisotropy, manuscript in preparation.

(21) Ezzat, S. S.; Mani, P. D.; Khaniya, A.; Kaden, W.; Gall, D.; Barmak, K.; Coffey, K. R. Resistivity and Surface Scattering of (0001) Single Crystal Ruthenium Thin Films. *J. Vac. Sci. Technol. A* **2019**, *37*, 031516.

(22) Milosevic, E.; Kerdsongpanya, S.; Zangiabadi, A.; Barmak, K.; Coffey, K. R.; Gall, D. Resistivity Size Effect in Epitaxial Ru(0001) Layers. *J. Appl. Phys.* **2018**, *124*, 165105.

(23) Barmak, K.; et al. Epitaxial Metals for Interconnects beyond Cu. *J. Vac. Sci. Technol. A* **2020**, *38*, 033406.

(24) Ye, J.; Thompson, C. V. Regular Pattern Formation through the Retraction and Pinch-off of Edges during Solid-State Dewetting of Patterned Single Crystal Films. *Phys. Rev. B - Condens. Matter Mater. Phys.* **2010**, *82*, 1.

(25) Ye, J.; Thompson, C. V. Anisotropic Edge Retraction and Hole Growth during Solid-State Dewetting of Single Crystal Nickel Thin Films. *Acta Mater.* **2011**, *59*, 582.

(26) Shin, Y. A.; Thompson, C. V. Templated Fingering during Solid State Dewetting. *Acta Mater.* **2021**, *207*, 116669.

(27) Cheynis, F.; Bussmann, E.; Leroy, F.; Passanante, T.; Müller, P. Dewetting Dynamics of Silicon-on-Insulator Thin Films. *Phys. Rev. B* **2011**, *84*, 245439.

(28) Bollani, M.; et al. Templated Dewetting of Single-Crystal Sub-Millimeter-Long Nanowires and on-Chip Silicon Circuits. *Nat. Commun.* **2019**, *10*, 1.

(29) Wulff, G. XXV. Zur Frage Der Geschwindigkeit Des Wachsthums Und Der Auflösung Der Krystallflächen. *Z. Für Krist. - Cryst. Mater.* **1901**, *34*, 449.

(30) Tran, R.; Xu, Z.; Radhakrishnan, B.; Winston, D.; Sun, W.; Persson, K. A.; Ong, S. P. Surface Energies of Elemental Crystals. *Sci. Data* **2016**, *3*, 1.

(31) Cahn, J. W.; Hoffman, D. l. A Vector Thermodynamics for Anisotropic Surfaces-II. Curved and Faceted Surfaces. *Acta Metall.* **1974**, *22*, 1205.

(32) Sekerka, R. F. *Thermal Physics*; Elsevier: Amsterdam, 2015.

(33) Taylor, J. E. II-Mean Curvature and Weighted Mean Curvature. *Acta Metall. Mater.* **1992**, *40*, 1475.